

Ages and Metallicities of Globular Clusters in NGC 4472

M.A. Beasley,^{1*} R.M. Sharples,¹ T.J. Bridges,² D.A. Hanes,³ S.E. Zepf,⁴ K.M. Ashman,⁵
D. Geisler,⁶

¹*Department of Physics, University of Durham, Durham DH1 3LE, UK*

²*Anglo-Australian Observatory, P.O. Box 296, Epping, NSW, 2121, Australia*

³*Department of Physics, Queen's University, Kingston, ON K7L 3N6, Canada*

⁴*Department of Astronomy, Yale University, New Haven, CT 06520*

⁵*Department of Physics and Astronomy, University of Kansas, Lawrence KS 66045*

⁶*Departamento de Física, Grupo de Astronomía, Universidad de Concepción, Casilla 160-C, Concepción, Chile*

ABSTRACT

We have derived ages and metallicities from co-added spectra of 131 globular clusters associated with the giant elliptical galaxy NGC 4472. Based upon a calibration with Galactic globular clusters, we find that our sample of globular clusters in NGC 4472 span a metallicity range of approximately $-1.6 \leq [\text{Fe}/\text{H}] \leq 0$ dex. There is evidence of a radial metallicity gradient in the globular cluster system which is steeper than that seen in the underlying starlight. Determination of the *absolute* ages of the globular clusters is uncertain, but formally, the metal-poor population of globular clusters has an age of 14.5 ± 4 Gyr and the metal-rich population is 13.8 ± 6 Gyr old. Monte Carlo simulations indicate that the globular cluster populations present in these data are older than 6 Gyr at the 95% confidence level. We find that within the uncertainties, the globular clusters are old and coeval, implying that the bimodality seen in the broadband colours primarily reflects metallicity and not age differences.

Key words: galaxies: individual: NGC 4472 – galaxies: elliptical – galaxies: star clusters

1 INTRODUCTION

It has become clear in recent years that subpopulations in extragalactic globular cluster systems (GCS) are not uncommon. Indeed, since their first detection by Zepf & Ashman (1993) using colour data from Couture, Harris & Allwright (1991) and Harris *et al.* (1992), the study of colour bimodality in GCSs has become a growth industry (e.g. Neilsen & Tsvetanov 1999; Gebhardt & Kissler-Patig 1999). It is now estimated that *at least* half of all early-type systems have bimodal GCSs (Gebhardt & Kissler-Patig 1999). What is not so clear is the origin of these subpopulations, and their implications for the formation of their host galaxies. The apparent ubiquity of globular clusters in galaxies, and the homogeneity of their GCSs naturally leads one to conclude that they are intimately associated with, if not the epoch of galaxy formation, at least its major modes of star formation.

NGC 4472, the brightest elliptical galaxy in Virgo, is an excellent candidate for such GCS research and has consequently been the subject of extensive photometric studies (e.g. Cohen 1988; Couture *et al.* 1991; Geisler, Lee &

Kim 1996; Lee, Kim & Geisler 1998). This galaxy (Hubble type E2) plays host to some 6300 \pm 1900 globular clusters (Geisler *et al.* 1996) which have been shown to possess a bimodal colour distribution (Zepf & Ashman 1993; Geisler *et al.* 1996). Adopting a distance modulus of $m - M = 31.0$, gives an absolute magnitude of $M_V = -22.6$ for this galaxy, and a specific frequency of $S_N = 5.6 \pm 1.7$ (Geisler *et al.* 1996).

To first order, the GCS colour distributions are thought to reflect the distribution of metallicity in the globular cluster populations (Ashman & Zepf 1998). Since globular clusters are generally thought to be old, their relative ages will not significantly affect broadband colours owing to the well known age-metallicity degeneracy (Faber 1972; O'Connell 1976; Worthey 1994). The problem of breaking this degeneracy, and extracting relative age information about globular cluster subpopulations has led to several avenues of investigation. One technique has been to compare broadband colours (which are primarily metallicity-sensitive) with magnitudes (which are largely age sensitive, assuming a given mass-to-light ratio). Puzia *et al.* (1999) have investigated the ages of the globular cluster subpopulations in NGC 4472, using HST *V* and *I* band photometry to determine both mean

* email: m.a.beasley@durham.ac.uk

colours and turn-over magnitudes. By assuming that the mean mass functions of the two subpopulations are similar, they find that the blue and red globular clusters are coeval within their uncertainties (which are ± 3 Gyr). They conclude that possibility of one population being half the age of the other is excluded at the 99% confidence level. However, Lee & Kim (2000) have also analysed HST *V* and *I* data for NGC 4472, using three datasets in common with the Puzia *et al.* (1999) study, and arrive at a different conclusion. They indicate that the red globular clusters are several Gyr *younger* than the blue globulars. This difference from the Puzia *et al.* (1999) study they attribute to a combination of a $\sim 30\%$ larger sample size, greater areal coverage and increased completeness. A similar result has been found by Kundu *et al.* (1999) for globular clusters in the inner regions of NGC 4486 (M87). They find that the red globular clusters are 3–6 Gyr younger than their blue counterparts, with the magnitude of the age difference dependent upon the stellar evolutionary models they adopt.

An alternative method is via spectroscopy, which can provide a way of disentangling age from metallicity through the careful selection of absorption-line indices. This approach circumvents the requirement of assumptions of a universal mass distribution for GCs. Metallicities may be directly measured from metal-sensitive features, and ages may be found from Balmer indices, which effectively measure the temperature of the main-sequence turnoff in globular clusters. In a previous paper, Sharples *et al.* (1998) obtained spectra for 47 globular clusters associated with NGC 4472, and including data from the study of Mould *et al.* (1990), found evidence for kinematical differences between the blue and red cluster populations. Another 100 spectra for *bona fide* globular clusters associated with this galaxy have now been obtained with the Multi-Object Spectrograph (MOS) at the 3.6-m Canada-France-Hawaii telescope (CFHT), creating a total dataset of 131 confirmed globular clusters. The kinematic analysis of these data is presented in Zepf *et al.* (in preparation), in this paper we concentrate on the abundances and ages of the NGC 4472 globular clusters.

The structure of this paper is as follows: in §2 we briefly overview previous spectroscopy for extragalactic GCSs in luminous ellipticals and in §3 the observations and data reduction are described. This is followed in §4 by the procedure for measuring line-strengths of the globular clusters. In §5 we present both the qualitative and quantitative results from this work. We discuss the implications of our findings in §6 and summarize our work in §7.

2 PREVIOUS SPECTROSCOPY OF GCS IN LUMINOUS ELLIPTICAL GALAXIES

The faintness of extragalactic GCS and the demands of spectroscopic studies upon instrumentation and telescope time have led to a situation where only a few line-strength measurements have been successfully undertaken for globular clusters outside the Local Group. Hanes & Brodie (1986) derived a mean metallicity of the M87 globular cluster system of $[\text{Fe}/\text{H}] = -0.5 \pm 0.4$ dex utilising low S/N and moderately low resolution integrated spectra. This is consistent with a value of $[\text{Fe}/\text{H}] = -0.89 \pm 0.16$ dex found by Brodie & Huchra (1991) using the MMT spectrograph at ~ 9.0 Å

resolution. Mould *et al.* (1990) use the median Mg *b* index and calibrations of Burstein *et al.* (1984) in order to obtain a mean metallicity of -1.0 ± 0.2 dex for M87 and -0.8 ± 0.3 dex for NGC 4472. More recently, Kissler-Patig *et al.* (1998) used the Keck telescope to obtain 5.6 Å resolution spectra of 21 globular clusters belonging to NGC 1399, the central cD galaxy of the Fornax cluster. They derive a mean $[\text{Fe}/\text{H}]$ of -0.8 dex and find that the elemental abundances of the majority of the globular clusters do not differ from those observed in the Milky Way and M31. However, two of their globular clusters stand out in that their metallic line indices are comparable to the diffuse stellar light of the host galaxy, perhaps implying that they may have formed from nearly solar metallicity gas in a different formation process from the bulk of the globular clusters (such as may be attributed to a merger event). They also exhibit Balmer line indices ($\text{H}\beta$, $\text{H}\gamma$) incompatible with *any* age-metallicity combination of existing stellar population models. Cohen, Blakeslee & Ryzhov (1998) analyse a larger sample of 150 globular clusters in M87, and show that the cluster system spans a wide range of metallicity, $-2.2 < [\text{Fe}/\text{H}] < 0.1$, dex with a mean $[\text{Fe}/\text{H}]$ of -0.95 dex. They find marginal evidence for a bimodal as opposed to unimodal metallicity distribution at the 86 % significance level, with 'peaks' at -1.3 and -0.7 dex, however this may be largely due to their object selection biases. Through the measurement of $\text{H}\beta$ and $\text{H}\alpha$ indices, they obtain a median age for the M87 GCS of 13 ± 2 Gyr, similar to that of the Milky Way globular clusters.

3 OBSERVATIONS AND DATA REDUCTION

The data constituting our combined sample was obtained from two separate observing runs. Spectroscopic observations of 79 cluster candidates were taken with the Low-Dispersion Survey Spectrograph on the 4.2-m William Herschel Telescope (WHT) in April, 1994 (see Sharples *et al.* 1998 for further details of these observations and the data reduction). This has now been supplemented by spectra of 171 cluster candidates obtained using MOS on the CFHT in May, 1998. Object selection in both studies was based on Washington photometry of NGC 4472 globular cluster candidates published by Geisler *et al.* (1996). Five multislit masks were prepared using the MOS software provided at the CFHT, though only four were actually used. Slits were cut using the LAMA machine, with typically 40 \sim 45 objects per mask. One of the masks was centred on the nucleus of NGC 4472, with the other four being displaced by ~ 5.5 into the NE, NW, SE, and SW quadrants to obtain the best spatial coverage of the cluster system. Highest priority was given to candidates in the magnitude range $19.5 < V < 21.5$, although candidates were selected down to $V=22.5$. Table 1 gives the details of the masks, listing the number of candidates per mask, along with the number of spectroscopically confirmed globular clusters, background galaxies and foreground stars. A number of spectra yielded no reliable identification, due to insufficient signal-to-noise (S/N) and/or problematical sky-subtraction.

The B600 grism with dispersion $2.24 \text{ \AA pix}^{-1}$ was used, producing spectra with an instrumental resolution of $\sim 5.5 \text{ \AA}$ (330 kms^{-1}) and a useful spectral range of $3800 - 6500 \text{ \AA}$. The detector was a STIS 2048² chip, with readout noise

Table 1. Details of the mask setup and spectroscopic completeness for the CFHT observations.

Mask #	RA (1950.0)	DEC (1950.0)	Objects/Mask	Confirmed Globulars	Background Galaxies	Foreground Stars
Mask1	12 27 15.14	08 16 37.4	unused	unused	unused	unused
Mask2	12 27 01.69	08 12 36.3	47	22	4	2
Mask3	12 27 01.69	08 20 38.3	42	26	3	0
Mask4	12 27 27.06	08 20 38.4	42	31	3	2
Mask5	12 27 27.06	08 12 36.4	45	21	3	3

Table 2. Observing log for CFHT run.

Dates	May 16-19 1998
Telescope/Instrument	3.58m CFHT/MOS
Detector	2048 ² STIS-2
Dispersion (Resolution)	2.24 Å pix ⁻¹ (5.5 Å FWHM)
Wavelength Coverage	3800 - 6500 Å
Seeing	< 1''
Mean Airmass	1.1
Exposure times (NGC 4472)	6000s per mask

9.3 e⁻, noteworthy for its excellent performance in the blue (quantum efficiency $\sim 82\%$ at 4000 Å). Flat field and bias frames were taken at the beginning and end of each night, and the spectra were wavelength calibrated using frequent mercury arcs taken before and after the programme object frames. Table 2 lists the observational details for the CFHT run.

For velocity calibration, we have obtained long slit spectra for a number of radial velocity standard stars. In addition, we have taken integrated spectra of several Galactic Globular Clusters (GGCs) in order to calibrate metallicities. The spatial extent of these globular clusters on the sky (mean core radii ~ 40 arcsec) required us to synthesize an aperture in order to obtain a representative integrated spectrum. We have therefore scanned the cores of the globular clusters over a typical range of 90 arcsec. Combined with the WHT observations, this yields high S/N spectra (~ 500 at 5000 Å) of five GGCs in the metallicity range $-2.24 < [\text{Fe}/\text{H}] < -0.29$ dex with one overlap, namely NGC 6356. We summarize our calibration objects in Table 3.

The majority of the data reduction was performed using the package DOSLIT in IRAF together with other standard tasks. Object frames were trimmed and bias-subtracted, and any bad pixels were cleaned by interpolating across adjacent columns. A second-order polynomial fit to these data produced residuals of order ~ 0.1 Å in the wavelength calibration. The spectra were then optimally extracted and sky-subtracted using a linear least-squares fit to the background sky. Finally, the spectra were rebinned with a step size of 2 Å on to a logarithmic wavelength scale over the range 3800 – 5500 Å. The resultant spectra typically possessed S/N ratios of 4 – 10.

4 ANALYSIS

Table 3. Programme standard stars and GGCs for radial velocity and metallicity calibration.

ID	Object	Spectral Type	[Fe/H] _Z ¹
NGC 6341	GGC	F2	-2.24
NGC 7078	GGC	F3-4	-2.15
NGC 6205	GGC	F6	-1.65
NGC 6356	GGC	G3	-0.62
NGC 6553	GGC	G4	-0.29
HD 90861	Star	K2III	-
HD 102494	Star	G9IV	-
HD 112299	Star	F8V	-
HD 132737	Star	K0III	-
HD 171232	Star	G8III	-
HD 208906	Star	F8V-VI	-

¹ Abundances from Zinn (1985), henceforth denoted [Fe/H]_Z.

4.1 Radial Velocities

The Fourier cross-correlation task FXCOR was used for determining radial velocities from the spectra. The six velocity templates were de-redshifted by their literature values and then individually cross-correlated against each of the candidate cluster spectra. An 'r' value of 2.5 (Tonry & Davis 1979) was set as the lower threshold for reliable measurement; below this any velocities returned, however plausible, were removed from further analysis. The final velocities of the globular clusters were taken to be the mean velocity weighted by the cross-correlation peak height of each template. A heliocentric correction was then applied to these velocities. In addition to the formal errors returned by the cross-correlation task, an estimate of the uncertainties may be made from the overlap between common objects in different masks. Between the data from Sharples *et al.* (1998) and the CFHT velocities there are a total of 13 overlaps. The mean difference of the sample is -17 kms⁻¹ with an inferred velocity uncertainty for a single measurement of 78 kms⁻¹.

We take a velocity range $300 \leq V_h \leq 2000$ kms⁻¹ as being representative of globular clusters associated with NGC 4472, which has a heliocentric velocity of 961 kms⁻¹ (Sandage & Tammann 1981). This is consistent with the mean velocity of our globular cluster sample of 990 ± 26 kms⁻¹, which has a velocity dispersion of 314 kms⁻¹. See Zepf *et al.* (in preparation) for further analysis of the globular cluster kinematics.

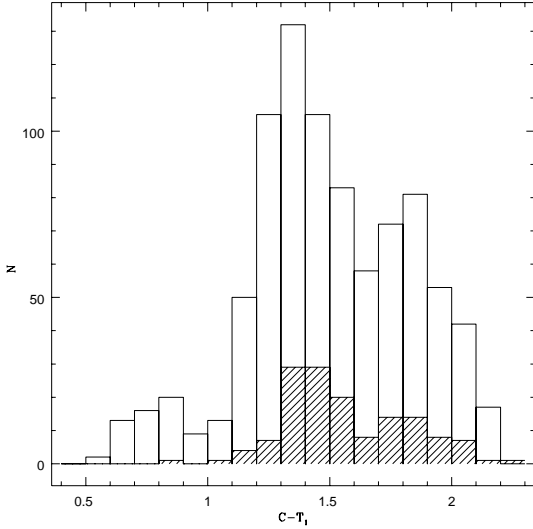


Figure 1. Colour distribution for globular cluster candidates with $19.5 \leq V \leq 22.5$ and $0.5 < C - T_1 < 2.2$ from Geisler *et al.* (1996). The open histogram is for the full sample of 860 candidates; the shaded histogram is for the 131 globular clusters for which radial velocities have been obtained.

4.2 Co-adding the Spectra

Whilst the quality of our individual spectra is adequate to obtain radial velocities, it is insufficient for reliable line-strength analysis. For any believable measurement of equivalent widths of absorption lines, a method of co-addition of the spectra was required so as to improve the S/N ratio.

Since the broadband colours of the globular clusters primarily reflect their metallicities (on the assumption that these are old stellar populations, $\tau \gtrsim 8$ Gyr), blue globular clusters should be metal-poor, and become progressively more metal-rich as they redden. The cluster spectra were therefore assigned bins on the basis of their $C - T_1$ colours from the photometry of Geisler *et al.* (1996). The globular cluster catalogue of Geisler *et al.* (1996) is bimodal in colour, and the subset of brightest globular clusters selected from this catalogue were chosen so as to reflect this bimodality, albeit with reduced cluster numbers. Fig. 1 shows the sample of 860 cluster candidates from Geisler *et al.* (1996) (open histogram) and those for which radial velocities have been obtained and subsequently used in the metallicity analysis (shaded histogram). Although we now have velocities for 141 globular clusters, 10 of these were from the original sample of Mould *et al.* (1990) and these spectra were unavailable for further analysis.

Due to this bimodality in these data, creating bins of a fixed width in colour leads to significantly different numbers of spectra in each bin. Spectra resulting from such binning are not readily comparable since their signal-to-noise (S/N) varies as a function of the number of spectra per bin. The bins were therefore constructed by assigning approximately equal numbers of spectra to each bin, yielding final spectra of similar S/N, but with different widths in colour. In order to determine the number of spectra per bin acceptable for reliably measuring line-strengths, the following procedure was adopted. The Spectral Energy Distributions (SEDs) of

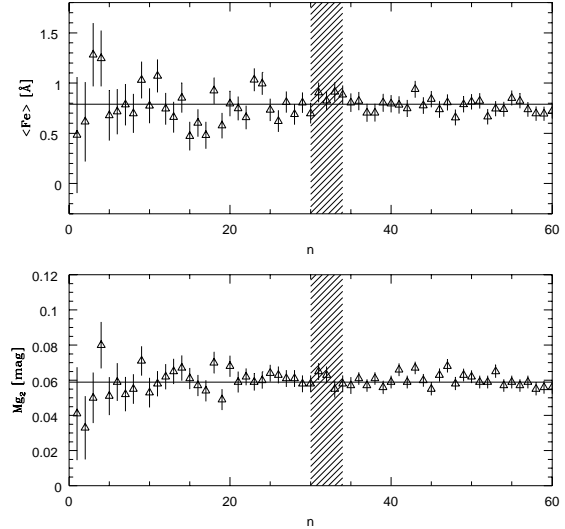


Figure 2. Line-strength measurements of $\langle \text{Fe} \rangle$ (top panel) and Mg_2 of the degraded and co-added SEDs of Worthey (1994). Each set of realisations is represented by an open triangle, with its associated statistical error. The shaded region indicates the location where the line-strength measurements were found to be stable. The solid horizontal line in each panel indicates the value of the index measurement for the original SED. Note that $\langle \text{Fe} \rangle$ is measured in units of Angstroms, whereas Mg_2 is expressed as a magnitude.

Worthey (1994) (see §5.2) at a fixed age and range of metallicities were degraded to the typical S/N of the NGC 4472 globular cluster spectra. This was achieved by adding random noise to the spectra until they possessed a distribution in S/N equivalent to that of the NGC 4472 globular cluster data. Subsequent spectra were then co-added and their line-strength indices measured (see §4.3 for discussion of index measurements). This process was reiterated until a sufficient number of realisations produced stable measurements in all indices, that were consistent with the indices measured for the original, undegraded spectrum.

An example of the results of this exercise is shown in Fig. 2 for the $\langle \text{Fe} \rangle^\dagger$ and Mg_2 indices. Each filled circle represents a set of n realisations, with their associated statistical errors, derived from the S/N of each spectrum obtained by summing over pixels along the slit within a fixed wavelength range ($\sim 4545 - 5500$ Å). The shaded column denotes where the number of co-added spectra were found to be sufficient to produce a stable index measurement. In this case, the degraded SED is that predicted by the Worthey (1994) models for a 17 Gyr stellar population with $[\text{Fe}/\text{H}] = -1.7$ dex. The indices measured from the co-added spectra (at $n = 32$) in Fig. 2 are 0.065 ± 0.011 mag for Mg_2 , and 0.85 ± 0.30 Å for $\langle \text{Fe} \rangle$, in excellent agreement with the models which predict 0.06 mag for and 0.79 Å for $\langle \text{Fe} \rangle$.

This procedure, repeated for different index features, showed no evidence of systematic effects. Initially, four

[†] $\langle \text{Fe} \rangle$ is defined as the mean of the Fe5270 and Fe5335 indices in González (1993).

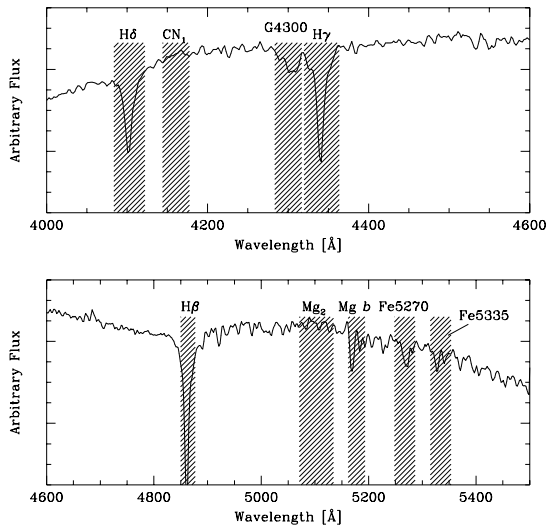


Figure 3. Location of the feature bandpasses measured in our data. Shaded regions show the width and position of the features, which are over-plotted on to the normalised spectrum of the metal-poor globular cluster M15.

colour bins where selected (set by the number of spectra required per bin), the first (bluest) consisting of 35 spectra, the remaining three each comprising of 32 spectra. Prior to co-addition, the spectra were transferred to the rest-frame using their measured radial velocities. This procedure is essential for any measurement of line indices using fixed-wavelength bandpasses (e.g. Brodie & Huchra 1990).

4.3 Line Indices

Numerous systems for measuring line-strengths in stellar populations exist, all with their respective merits and failings. However, the key features considered important here are the size and availability of the observational database, and the range of stellar models with which to calibrate these data. In this respect, the Lick system (Burstein *et al.* 1984; Faber *et al.* 1985; Gorgas *et al.* 1993) is our system of choice.

The absorption-line indices were measured following a prescription similar to that described in Brodie & Huchra (1990), which is based upon the Lick/IDS system of bandpasses as presented in Burstein *et al.* (1984). Each index is fully described by two pseudocontinuum regions and one feature bandpass region.

For atomic lines, the equivalent width is defined as:

$$EW = \int_{\lambda_1}^{\lambda_2} \left(1 - \frac{F_{I\lambda}}{F_{C\lambda}}\right) d\lambda \quad (1)$$

where λ_1, λ_2 are the wavelength limits of the passband, and $F_{I\lambda}, F_{C\lambda}$ are the flux per unit wavelength of the measured feature and the continuum respectively.

Molecular line-strengths are similarly defined, but are measured in magnitudes:

$$I = -2.5 \log \left[\left(\frac{1}{\lambda_2 - \lambda_1} \right) \int_{\lambda_1}^{\lambda_2} \frac{F_{I\lambda}}{F_{C\lambda}} d\lambda \right] \quad (2)$$

Table 4. Dependence of spectral resolution on wavelength for the Lick/IDS.

Wavelength [Å]	Resolution (FWHM) [Å]
4000	11.5
4400	9.2
4900	8.4
5400	8.4
6000	9.8

We have also measured two more Balmer indices, $H\gamma_A$ and $H\delta_A$, defined by Worthey & Ottaviani (1997). The subscript 'A' denotes the wider of their four indices (they also define $H\gamma_F$ and $H\delta_F$ which are ~ 20 Å wide) which were principally designed to measure the absorption from A-stars.

For comparison with the stellar population models of Worthey (1994), we use the index definitions given in Worthey *et al.* (1994) and Worthey & Ottaviani (1997). To compare with the empirical calibrations of Brodie & Huchra (1990), we also measure indices using the index definitions given in Brodie & Huchra (1990), which differ largely in their placing of the continuum. Fig. 3 illustrates the locations of the feature bandpasses measured in this study, the regions of pseudocontinua are omitted for clarity.

The Lick/IDS system is based upon a stellar library which is *not* flux-calibrated, and its resolution (FWHM) varies as a function of wavelength. Our data have a fixed spectral resolution of ~ 5.5 Å (FWHM) and have also not been flux-calibrated (due to the difficulties of fluxing multi-slit data). Consequently, it is difficult to accurately transform our measurements on to the Lick System and care must be taken, particularly with regard to the continuum slope (e.g. Worthey & Ottaviani 1997; Cohen *et al.* 1998).

The first step in approximating to the Lick system is to convert the resolution of our data to that of the IDS. In Table 4 we reproduce the data given in table 8 of Worthey & Ottaviani (1997), illustrating the dependence of spectral resolution upon wavelength for the IDS. For our multislit data, the useful spectral range is 3800 Å – 5500 Å, covering a Lick resolution from approximately 11.5 Å to 8.4 Å. We first divide our co-added spectra into 200 Å intervals, and the resolution required to best match the Lick/IDS spectra within that interval was taken from Table 4. Our spectra were then degraded from a resolution of $\delta\lambda_{N4472}$ to the IDS at $\delta\lambda_{IDS}$ by convolution with a Gaussian kernel of width σ , given according to Eqn. (3).

$$\sigma = \frac{\sqrt{(\delta\lambda_{IDS}^2 - \delta\lambda_{N4472}^2)}}{2.35 * \text{Å pix}^{-1}} \quad (3)$$

The indices of the unbroadened spectra were then compared to those of the Lick resolution spectra to check for any possible systematic differences. The broader indices were largely unaffected, for example Mg_2 , which has a width of 42.5 Å, was unchanged. However $Mg b$, a narrower index (width 32.5 Å) was systematically lower by approximately 0.14 Å when measured from the broadened spectra.

The second consideration is the effect of the instrumental response curve upon the continuum slope of the indices.

Table 5. Effect of the continuum shape on index measurements of features in HD 102494. For comparison purposes, we have converted the molecular indices CN₁ and Mg₂ into equivalent widths of absorption.

Feature	Mean [Å]	Median [Å]	σ [Å]	Width [Å]
CN ₁	0.193	0.289	0.42	35
G4300	3.017	2.986	0.10	35
H β	0.808	0.801	0.02	28.75
Mg ₁	0.358	0.297	0.54	65
Mg ₂	2.396	2.322	0.20	42.5
Mg <i>b</i>	1.542	1.545	0.02	32.5
Fe5270	1.335	1.399	0.02	40
Fe5335	0.982	0.984	0.01	40
H δ_A	-1.739	-1.694	0.19	38.75
H γ_A	-3.016	-3.041	0.10	43.75

We have simulated the effect of varying the local spectral slope of each feature bandpass, by altering the *global* continuum shape of the spectra. A polynomial was fitted to each of our co-added spectra, representing the full range of continuum shape in our data. This entire set of artificial ‘response functions’ were then added to a normalised standard spectrum and the indices of each were measured and the results compared. Table 5 shows the effect upon the index measurements resulting from this variation in the continuum.

As Table 5 indicates, the majority of the features remain relatively stable. However, it is apparent that the CN₁ and Mg₁ features are very sensitive to small shifts in the slope of the local continuum and cannot be trusted in these current data. To a lesser extent, Mg₂ and H δ_A are also susceptible to changes in the continuum level. In view of this we omit the CN₁ and Mg₁ from further analysis, and recognize the behaviour Mg₂ and H δ_A . We note that *extreme care must be taken when measuring indices under the Lick system if the continuum has not been corrected to that of the IDS. This is especially true for the broader features.*

Errors in the velocities of the individual spectra had no significant effect upon the line indices measured for our co-added spectra. Our uncertainties in the radial velocities velocities are $\leq 100 \text{ kms}^{-1}$, translating to approximately half a pixel at the resolution of our data. Similarly, we applied no correction for line broadening due to any *internal* velocity dispersion of the globular clusters. Internal stellar velocity dispersions of globular clusters are small, typically $\sim 10 \text{ kms}^{-1}$ or less (e.g. Meylan & Heggie 1997).

4.4 Uncertainties in the Indices

The value of any line-strength measurement is dependent upon a suitable calculation of the associated errors. For an old stellar population at roughly solar metallicity, an error as small as 0.2 Å in the Mg *b* index translates into an uncertainty of ~ 0.2 dex in metallicity, and an uncertainty of 0.2 Å in the H β index corresponds to an error of ~ 3 Gyr in age. The main sources of uncertainty in the index measurements of the co-added spectra stem from systematics in the binning process and any intrinsic spread in the chemical

composition of the globular clusters. The latter is inherent in these data; the spectra comprise of colour bins of a finite width which can only be adjusted through alterations in this binning. These uncertainties may be best estimated through the use of a bootstrap technique, which takes into account the stochastic nature of co-adding individual, low S/N spectra. The method we use is quite straightforward: each of our colour bins contain n spectra, and each spectrum is assigned a number from 1 to n . A spectrum is then selected randomly from the bin by its corresponding number and placed into a new pool which holds the spectra to be combined. This process is then repeated until the resulting in a pool contains n randomly selected spectra from the original bin. The spectra are selected *with replacement*, so the bin is never depleted and the new pool is likely to contain several repetitions of the same spectrum. The spectra contained within the pool are then combined to produce a final composite spectrum, which then has its line indices measured. This description comprises one realisation and is repeated many times so as to produce many index measurements of the same feature. Typically 150 realisations were performed for each colour bin. We take the final index value to be the mean of the distribution of measurements for each bin and its associated uncertainty as the standard deviation of this distribution. In addition, we have also measured the flux-weighted colours for each bin. This is preferable over a magnitude weighting scheme, since the amount of light received through each slit on to the detector is not only a function of an individual globular clusters’ brightness, but also of its position in the slit. Fig. 4 shows representative co-added spectra for the four colour bins, which have the mean flux-weighted colours of $C - T_1 = 1.30, 1.44, 1.61$ and 1.91 respectively. Metal lines clearly become progressively stronger with redder colours (e.g. Mg *b* feature at ~ 5180 Å), whilst the Balmer lines weaken (e.g. H β at 4860 Å and H γ_A at 4340 Å).

We have extensively tested the effects of altering the bin size for our globular cluster data. We have varied n , the number of spectra per bin, and repeated the above procedure determining the variance in the indices in each case. Fig. 5 shows the dependence of σ upon n for our co-added spectra. The uncertainties in all of the indices behave in a similar fashion, with a steep initial gain in accuracy of ~ 0.02 Å / spectrum, and then flattening considerably with increasing n . The uncertainties in the Mg₂ index are ~ 0.1 Å greater than for the other indices, which we largely attribute to its sensitivity to variations in the continuum slope. Fig. 5 indicates that we may expect an uncertainty in most of the indices of 0.3 Å – 0.4 Å and 0.5 Å (0.013 mag) in Mg₂ for $n \simeq 30$.

4.5 Results

The indices measured for the four cluster bins using the bandpass definitions in Worthey *et al.* (1994) and Worthey & Ottaviani (1997) are given in Table 6. Associated uncertainties obtained from the bootstrap are tabulated in alternate rows. Errors for the mean bin colour are the standard deviation of the distribution of the flux weighted $C - T_1$ colours from the bootstrap procedure. Column 3 of Table 6 gives the metallicities predicted by the $C - T_1$ colours using the linear relation of Geisler & Forte (1990):

Table 6. Measured indices for our four colour bins of NGC 4472 globular clusters. Column 2 gives the flux weighted mean $C - T_1$ colour for the bin. The metallicity given in column 3 is derived from these colours using Eqn. (4), the relation of Geisler & Forte (1990) and is henceforth denoted $[\text{Fe}/\text{H}]_{\text{GF}}$. Uncertainties derived from the bootstrap are given in alternate rows.

Bin	$C - T_1$ [mag]	$[\text{Fe}/\text{H}]_{\text{GF}}$ (dex)	G4300 [Å]	$H\beta$ [Å]	Mg_2 [mag]	$Mg\ b$ [Å]	Fe5270 [Å]	Fe5335 [Å]	$H\delta_A$ [Å]	$H\gamma_A$ [Å]
1	1.30	-1.34	2.030	2.452	0.072	1.648	1.573	1.093	2.497	0.374
...	± 0.09	0.21	0.397	0.330	0.011	0.303	0.275	0.274	0.815	0.566
2	1.44	-1.00	3.590	1.956	0.114	2.287	1.778	0.942	-0.466	-1.607
...	± 0.07	0.16	0.550	0.430	0.011	0.295	0.436	0.317	1.346	0.582
3	1.61	-0.61	4.017	1.630	0.126	2.115	1.706	1.432	0.018	-2.763
...	± 0.06	0.14	0.469	0.244	0.008	0.206	0.289	0.179	0.896	0.753
4	1.91	0.10	6.417	1.225	0.240	4.347	3.195	2.770	-2.052	-6.354
...	± 0.11	0.26	0.943	0.410	0.019	0.359	0.331	0.468	1.913	1.658

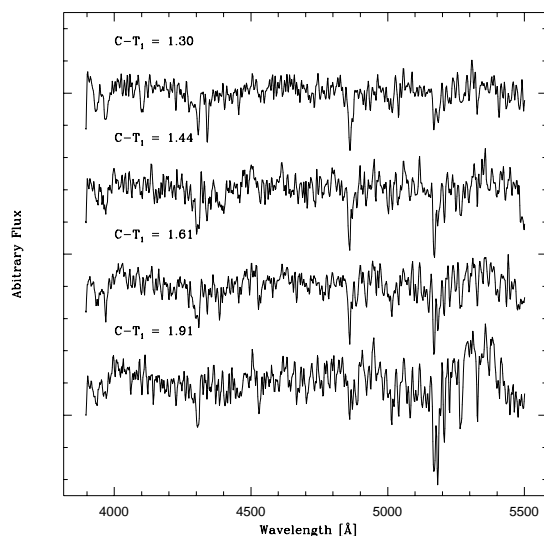


Figure 4. Representative co-added spectra of the globular clusters obtained from the bootstrap procedure. The spectra become progressively redder from top to bottom. The mean colours in $C - T_1$ are 1.30, 1.44, 1.61 and 1.91 respectively. The spectra have been divided through by a fifth-order polynomial, and have been shifted in the y -axis for clarity.

$$[\text{Fe}/\text{H}] = 2.35 * (C - T_1) - 4.39 \quad (4)$$

Eqn. (4) is based upon a calibration of 48 GGCs using the photometry of Harris & Canterna (1977) and $[\text{Fe}/\text{H}]$ values from Zinn (1985) and Armandroff & Zinn (1988). The range of metallicity spanned by this calibration is $-2.5 < [\text{Fe}/\text{H}] < -0.25$ dex.

5 GLOBULAR CLUSTER METALLICITIES AND AGES

5.1 Fiducial Globular Clusters

As a quantitative comparison, and in order to calibrate the stellar population models that we will use for obtaining abundances and ages, we have obtained trailed, long-slit integrated spectra for five GGCs. We supplement this

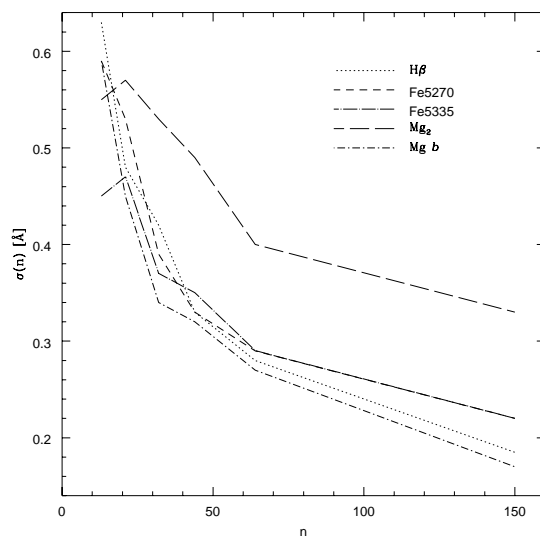


Figure 5. The dependence of the variance in the measured indices of the co-added spectra, upon the number of spectra per bin.

with data from Brodie & Huchra (1990) and Cohen *et al.* (1998). The measured Lick indices for our combined WHT and CFHT sample of GGCs are given in Table 7. Zinn (1985) quotes a typical uncertainty in the metallicities of the GGCs (column 11 in Table 7) of 0.15 dex.

In Figs. (6 – 9) we plot our co-added NGC 4472 data together with the combined sample of GGCs for which we have line-strength measurements. The linear fits in the figures applied to our data are not physically motivated, but merely serve as a comparison to the GGCs. Inspection of these figures reveals several points. As expected, the $H\beta$ index increases with the decreasing strength of the more metallicity-sensitive lines. The co-added cluster data of NGC 4472 falls within the metallicity and age ranges of the GGCs. The metal-rich ends of these data coincide at approximately solar, but the GGCs extend out to much lower metallicities. The mean line of the NGC 4472 globular clusters traces that of the GGC distribution fairly closely. The index-index plots in Fig. 8 and Fig. 9 are well-correlated with each other, with no obvious evidence of systematic offsets between the differ-

Table 7. Measured Lick/IDS indices for GGCs from the WHT and CFHT observing runs. Uncertainties are derived from the quadrature sum of the Poisson statistics and the rms between overlapping measurements.

ID	Run	G4300 [Å]	H β [Å]	Mg ₂ [mag]	Mg <i>b</i> [Å]	Fe5270 [Å]	Fe5335 [Å]	H δ_A [Å]	H γ_A [Å]	[Fe/H] _Z (dex)
NGC 6341	WHT	0.83	2.63	0.013	0.56	0.47	0.34	3.94	2.37	-2.24
...	...	± 0.72	0.05	0.009	0.07	0.15	0.03	0.13	0.19	...
NGC 7078	CFHT	0.37	3.10	0.018	0.53	0.96	0.37	4.71	3.43	-2.15
...	...	± 0.06	0.03	0.002	0.04	0.04	0.04	0.07	0.06	...
NGC 6205	WHT	2.14	2.31	0.045	1.00	0.92	0.78	3.17	0.71	-1.65
...	...	± 0.82	0.08	0.003	0.12	0.02	0.05	0.13	0.13	...
NGC 6356	CFHT	4.98	1.73	0.151	3.13	1.80	1.61	-0.52	-3.79	-0.62
...	...	± 0.38	0.19	0.011	0.09	0.11	0.10	0.16	0.15	...
NGC 6356	WHT	4.72	1.57	0.174	3.16	1.94	1.49	0.08	-3.80	-0.62
...	...	± 0.20	0.17	0.012	0.08	0.11	0.12	0.10	0.09	...
NGC 6553	CFHT	5.08	1.55	0.244	4.11	3.13	2.38	-0.90	-5.59	-0.29
...	...	± 0.17	0.30	0.002	0.15	0.04	0.07	0.18	0.21	...

ent indices. Although there is only one overlap between the two observing runs, namely NGC 6356, the agreement is good in this case. Five of our GGCs are in common with the combined dataset of GGCs from Brodie & Huchra (1990) and Cohen *et al.* (1998), and in most cases these data are in good agreement. However, our measurement of H β for NGC 7078 (M92) is $\sim +0.5$ Å offset from the value measured by Cohen *et al.* (1998), and the reason for this is unclear.

In summary: the reddest bin of our globular clusters has a similar metallicity to the most metal-rich GGCs. The bluest bin is significantly more metal-rich than the bluest GGCs. The indices act together in the expected sense, metal-lines strengthen towards the red and the Balmer indices weaken. The co-added data are self-consistent within the bootstrapped uncertainties, which gives us confidence in our data and error estimates.

5.2 SSP models

To derive the ages and metallicities of the NGC 4472 globular clusters, we compare our data with single age, single metallicity stellar population models (SSPs). These model aggregates of coeval stars with homogeneous metal content, i.e. an idealised globular cluster. The SSP models considered here are the on-line versions of Worthey (1994) which can come in several variants, and may be fine-tuned from the web-page of Dr. Worthey.[‡] For our purposes, we restrict ourselves to models with a Salpeter initial mass function, with the assumption of a single, instantaneous burst of star formation. However, the grids used in this study differ from the original Worthey (1994) models in one important respect, which is in their treatment of the horizontal branches (HBs) for metal-poor globular clusters. The morphology of the HB now follows the observed behaviour of the GGCs, in that they become more extended toward the blue for more metal-poor globular clusters, as opposed to assuming a red clump at the base of the HB irrespective of metallicity. The GGCs M3 and M92 were used as templates for this behaviour (e.g. Aaronson *et al.* 1978 - for further discussion

[‡] <http://astro.sau.edu/~worthey/>

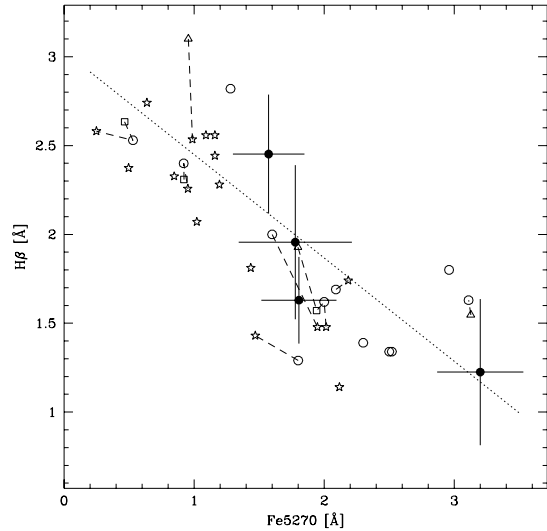


Figure 6. H β index as a function of Fe5270. Solid circles with error bars are for the co-added NGC 4472 cluster data. Open symbols are GGCs: CFHT - triangles, WHT - squares, circles indicate the data of Cohen *et al.* (1998) and stars represent data from Brodie & Huchra (1990). Dashed lines join globular clusters common between the datasets. The dotted line indicates the formal linear fit to our co-added NGC 4472 data.

see Worthey 1993). This change significantly increases the predicted H β index by upwards of 0.5 Å at [Fe/H] \leq -0.5 dex. Fig. 10 illustrates this effect and its importance with regard to the predicted ages for globular clusters, of which a substantial population have sub-solar abundances. A globular cluster with a measured Fe5270 index of 1.5 Å and H β index of 2.4 Å would be assigned an age of 8 Gyr according to the old models, but is predicted to be \geq 17 Gyr old by the models using the new HB morphology.

As a case in point, it is interesting to compare the H β indices of GGCs at the same metallicity, but with differing HB morphologies. One of our calibrating GGCs is M13 (NGC 6205), for which we have measured H β = 2.40 Å, and has a HB ratio of approximately unity (effectively it has the

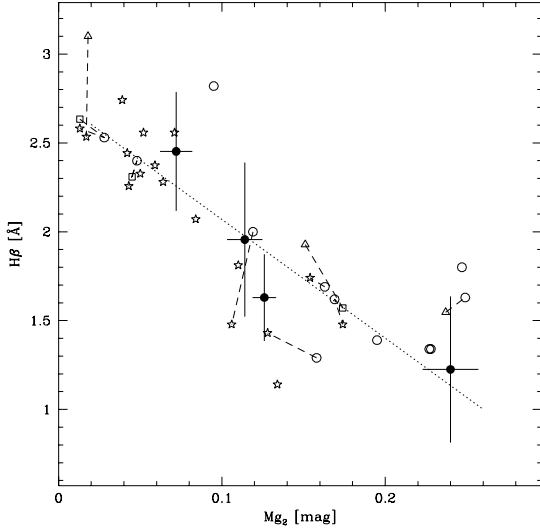


Figure 7. The $H\beta$ index against Mg_2 . Symbols are the same as for Fig 6.

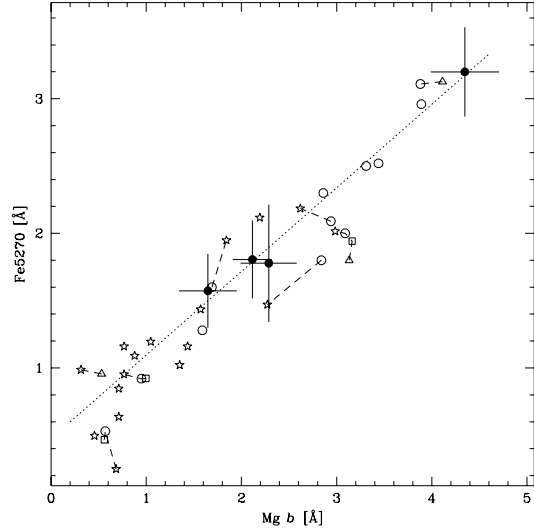


Figure 9. Fe5270 index versus $Mg b$. Symbols are the same as for Fig 6.

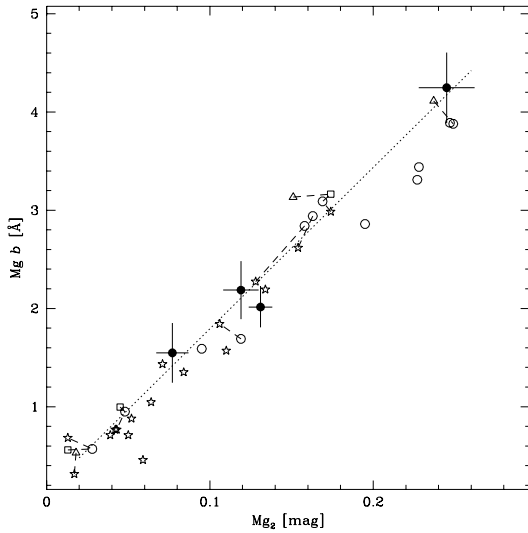


Figure 8. The $Mg b$ index as a function of Mg_2 . Symbols are the same as for Fig 6.

same number of stars both blueward and redward of the RR Lyrae gap). Amongst the sample of Cohen *et al.* (1998) is the GGC M3 (NGC 5272), for which they obtain $H\beta = 2.31 \text{ \AA}$, and has an extremely blue HB. Since both of these GGCs have $Fe/H \sim -1.65$, this would imply that HB morphology has little or no effect upon $H\beta$, contrary to the predictions of the above SSP models. Clearly, a high quality, homogeneous data set is required to investigate whether the horizontal branch may affect the Balmer indices of globular clusters at the same metallicity.

The model grids cover a metallicity-age parameter space of $-0.5 \leq [Fe/H] \leq 0.5$ with isochrones of $1.5 \leq \tau \leq 17$ Gyr. To cover old, metal-poor populations, they have been subsequently extended to bracket $-2.0 \leq [Fe/H] \leq 0.5$ for

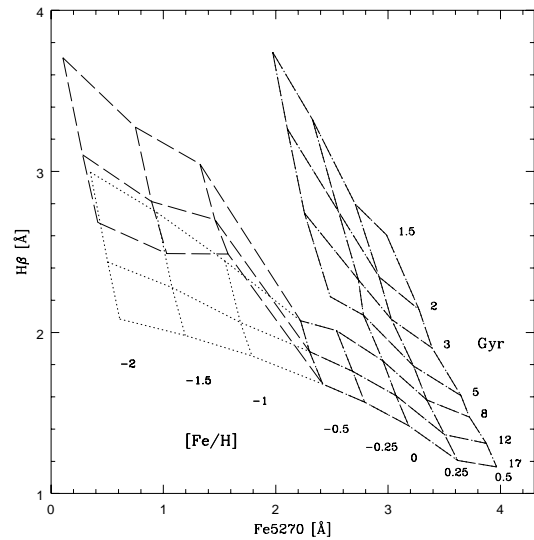


Figure 10. Effect of horizontal branch morphology on the Fe5270– $H\beta$ grid of the SSP models of Worthey (1994). The horizontal scale indicates the positions of constant lines of metallicity (running almost vertically here), ranging from 1/100 to 3 times solar. The approximately horizontal grid lines represent isochrones ranging from 1.5 to 17 Gyr (read from top to bottom). Faint dotted lines indicate the predictions of the original models assuming a red clump, long dashed lines show the result of including extended HBs following the observed behaviour of GGCs.

ages $8 \leq \tau \leq 17$ Gyr. The orthogonality of the index-index plots indicates the degree of decoupling between age and metallicity in the models.

The assumption of a red clump in the Worthey (1994) models possibly explains the findings of Cohen *et al.* (1998) that formally their metal-rich GGCs are *older* than the metal-poor ones, the opposite of what one might expect.

This new treatment of the HBs in the models predicts similar ages for the metal-rich and metal-poor GGCs.

5.3 Model Predictions

5.3.1 Metallicities of the Globular Clusters

We calibrate the SSP models using the indices measured for the combined sample of GGCs. The metallicities predicted by the models of Worthey (1994) must first be placed on to the metallicity scale of our GGCs. We use the most widely used metallicity scale for GGCs, which is that of Zinn (1985). This is primarily based on a number of narrow-band photometric indices sensitive to the ultraviolet blanketing in the integrated light of the globular cluster spectral energy distribution. Whilst there is increasing evidence that this metallicity scale is non-linear (e.g. Carretta & Gratton 1997), we adopt it since it remains self-consistent and the empirical calibrations of Brodie & Huchra (1990) are based upon this (see below).

We first obtain $[\text{Fe}/\text{H}]$ on the Worthey (1994) scale as a function of the Fe5270, Mg *b* and Mg₂ indices for our entire sample of GGCs. The newly assigned metallicities for the globular clusters are then compared to those of Zinn (1985) in order to derive a transformation function from the model metallicities to that of the Zinn (1985) metallicity scale. The G4300 and Fe5335 indices are not used for the re-scaling of the models, since there are fewer GGCs with measurements of these indices. For the magnesium indices, we obtain the linear transformations:

$$[\text{Fe}/\text{H}]_z = 0.631 * [\text{Fe}/\text{H}]_{\text{Mg } b} - 0.349, \sigma = 0.19 \text{ dex} \quad (5)$$

$$[\text{Fe}/\text{H}]_z = 0.799 * [\text{Fe}/\text{H}]_{\text{Mg}_2} - 0.230, \sigma = 0.16 \text{ dex} \quad (6)$$

for Mg *b* and Mg₂ respectively.

The Fe5270 index proved to be non-linear, and was fit with the quadratic:

$$[\text{Fe}/\text{H}]_z = -0.186 + 0.406 * [\text{Fe}/\text{H}]_{\text{Fe}} - 0.393 * [\text{Fe}/\text{H}]_{\text{Fe}}^2 \quad (7)$$

with an rms of $\sigma=0.2$ dex.

We now derive metallicities from the model predictions for our co-added data using the mean[§] of the Fe5270, Mg *b* and Mg₂ indices, transformed on to the Zinn (1985) scale as described above; we do not use the Balmer lines in this determination. We assign weights to each index, corresponding to the inverse of the scatter from Eqns. (5 – 7). Table 8 lists the metallicities determined for our four mean globular cluster spectra. We then compare these metallicities with those predicted by the empirical calibrations of Brodie & Huchra (1990). Their relations between the metallicity scale of Zinn (1985) and line-strength indices of integrated spectra are based upon observations of globular clusters in the Milky Way and M31. They identify six primary calibrators for metallicity in old stellar populations, two of which (namely Mg₂ and Fe5270) we have reliably measured in this study. We take the metallicity derived from this calibration as the

[§] Strictly speaking, the indices should be averaged *linearly*, whereas the commonly used metallicity indicator $[\text{Fe}/\text{H}]$ is expressed as a logarithmic scale. However, the difference between the two was only at the level of $\sim 1\%$, significantly less than the measurement error.

Table 8. Metallicities for our co-added NGC 4472 globular clusters using the predictions of the Worthey (1994) models (denoted $[\text{Fe}/\text{H}]_W$) and the empirical calibrations of Brodie & Huchra (1990) (denoted $[\text{Fe}/\text{H}]_B$). We also show the metallicities predicted from the $C - T_1$ colours using Eqn. (4). Uncertainties in the metallicities are tabulated in alternate rows.

Bin	$[\text{Fe}/\text{H}]_W$	$[\text{Fe}/\text{H}]_B$	$[\text{Fe}/\text{H}]_{GF}$
1	-1.29	-1.3	-1.34
...	± 0.3	0.21	0.21
2	-0.91	-1.03	-1.00
...	± 0.35	0.31	0.16
3	-0.84	-0.97	-0.61
...	± 0.25	0.21	0.14
4	-0.27	0.30	0.10
...	± 0.30	0.30	0.26

mean predicted by the Mg₂ and Fe5270 indices measured from our spectra, weighted by the reciprocal uncertainty in the index.

The metallicity predictions of the models are generally in good agreement with the primary calibrators of Brodie & Huchra (1990). However, the models predict that our reddest bin is ~ 0.6 dex more metal poor than the value derived from the Brodie & Huchra (1990) calibration. Kissler-Patig *et al.* (1998) indicate a similar phenomenon for metal-rich globular clusters in NGC 1399. They find that for Mg₂ > 0.180 mag, the linear extrapolation of Brodie & Huchra (1990) differs noticeably from their metal-rich globular clusters. Applying the correction employed by Kissler-Patig *et al.* (1998) to our data assigns our reddest cluster bin $[\text{Fe}/\text{H}] \sim -0.2$, thus bringing the metallicity into line with the model predictions. The metallicities derived from the flux-weighted Washington colours using Eqn. (4) compare well to the predictions of the Worthey (1994) models, although again they tend to give slightly higher metallicities for the redder two bins.

Our cluster bins have a metallicities of approximately $-1.6 \leq [\text{Fe}/\text{H}] \leq 0$, which is the range covered by the most metal-rich two-thirds of the Milky Way globular clusters. Clearly this is truncated due to the binning of the globular clusters; the actual colour distribution of the globular clusters from the Geisler *et al.* (1996) catalogue infers a metallicity range from one thousandth to ten times solar. At the metal-poor and metal-rich ends, this is extrapolated beyond the range covered by GGCs from which the colour- $[\text{Fe}/\text{H}]$ relation was derived, and therefore carries a greater uncertainty (e.g. Harris *et al.* 1992). Our bluest and reddest cluster bins correspond approximately with the bimodal peaks of the NGC 4472 globular cluster metallicity distribution.

The agreement between the metallicities predicted by the SSP models with those derived from the empirical calibration and flux-weighted colours is encouraging, and gives us some confidence in the model predictions. Since we will use the SSP models in the age determination of the globular clusters, we assign the metallicities predicted by the models to our globular cluster data as opposed to the mean metallicity given by the different methods.

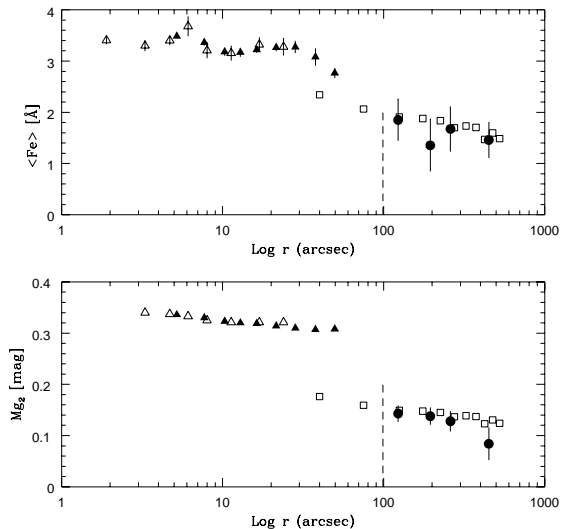


Figure 11. The behaviour of the $\langle\text{Fe}\rangle$ and Mg_2 indices (upper and lower panels respectively) with the logarithm of the projected galactocentric radius. Solid circles represent our co-added NGC 4472 globular clusters with their respective bootstrapped uncertainties. The open squares are the predicted index values for NGC 4472 globular clusters from the photometry of Geisler *et al.* (1996) (see text). We also plot the nuclear data of Davies *et al.* (1993), both for the Cryogenic camera (solid triangles) and the Texas Instruments CCD (open triangles). The dashed line indicates the effective radius of NGC 4472 ($r_e \sim 99$ arcsec).

5.3.2 Radial Gradients in the Globular Cluster Populations

Geisler *et al.* (1996) found a radial gradient in the mean $C - T_1$ colours of the NGC 4472 globular clusters corresponding to $\Delta[\text{Fe}/\text{H}]/\Delta\log r \simeq -0.4$ dex/log (arcsec), $\sigma \sim 0.2$ dex. This they primarily attributed to the varying spatial concentration of the blue and red cluster populations, in the sense that the ratio of blue to red globular clusters increases as a function of galactocentric radius. They also found that the mean colours of the red globular clusters were similar to that of the spheroid light, whilst the colours of the blue population were bluer than the galaxy light by ~ 0.5 mag at all radii.

We now investigate how the line-strengths of the NGC 4472 globular clusters behave as a function of projected galactocentric radius. We first separate our globular cluster data into four radial bins, and measure their mean line-strength indices. Our spectroscopic sample spans a range of galactocentric radii of $65 \leq r \leq 569$ arcsec ($0.5 \leq r_e \leq 6$), where $r_e = 99$ arcsec, which is the effective radius of NGC 4472 (Davies, Sadler & Peletier 1993). To ensure that any detected radial gradient does not originate from a varying spatial distribution in the globular cluster subpopulations, we fix the ratio of blue:red globular clusters for each bin (we define the red globular clusters as those having $C - T_1 \geq 1.625$). Since the global ratio of blue to red globular clusters in this study is $\sim 2:1$, the number of red globular clusters per bin effectively sets our limiting bin size. In Fig. 11 we plot $\langle\text{Fe}\rangle$ and Mg_2 measured for our data against the logarithm of their mean galactocentric radii.

We also show in Fig. 11 line-strengths of the spheroid light of NGC 4472, taken from Davies *et al.* (1993), who have measured the Mg_2 and $\langle\text{Fe}\rangle$ indices out to $\sim 0.5 r_e$ for this galaxy. To link the radial ranges covered by our data with that of Davies *et al.* (1993) more completely, we have converted the $C - T_1$ colours of the radially binned NGC 4472 globular clusters from Geisler *et al.* (1996) using Eqn. (4) and the empirical relations of Brodie & Huchra (1990). For clarity we have omitted the error bars on the converted photometry, but typically the uncertainty in $\langle\text{Fe}\rangle$ is ~ 0.4 Å and in Mg_2 is ~ 0.03 mag. The conversion from $C - T_1$ to $\langle\text{Fe}\rangle$ is not a direct one, since Brodie & Huchra (1990) calibrated Fe5270 with metallicity, as opposed to the mean of the Fe5270 and Fe5335 indices. We have applied a correction of 0.3 Å to convert the Fe5270 prediction to $\langle\text{Fe}\rangle$.

The converted globular cluster colour data of Geisler *et al.* (1996) is in good agreement with our $\langle\text{Fe}\rangle$ line-strengths at all radii. A shift of ~ 0.5 dex in $\langle\text{Fe}\rangle$ (corresponding to removing the blue globular clusters) would make these data overlap with that of the nuclear line-strength measurements. The metal-rich globular clusters appear to have similar iron abundances to the spheroid light. However, the situation for Mg_2 appears somewhat different. Again, our data are consistent with the indices predicted by the globular cluster photometry of Geisler *et al.* (1996). However, the GCs are offset downwards from the spheroid data of Davies *et al.* (1993) by ~ -0.10 mag at the same radii. Assuming the data of Geisler *et al.* (1996) traces the behaviour of the GCs inwards to $0.5 r_e$, then even after applying an additive shift of 0.05 mag (for the metal-rich GCs), there is still a difference of ~ 0.05 mag between the GCs and spheroid light.

It is evident that there is a metallicity gradient in our co-added data, in the sense that Mg_2 and $\langle\text{Fe}\rangle$ weaken with increasing galactocentric radius. We see no significant trend of changing flux in the spectra with radius, which could possibly introduce an artificial radial gradient. Applying a weighted linear fit to the $\langle\text{Fe}\rangle$ and Mg_2 indices, we obtain $\Delta[\text{Fe}/\text{H}]/\Delta\log r = -0.30 \pm 0.21$ dex for $\langle\text{Fe}\rangle$ and $\Delta[\text{Fe}/\text{H}]/\Delta\log r = -0.94 \pm 0.31$ for Mg_2 . The steep gradient seen in Mg_2 is primarily driven by the outermost radial bin (which has the largest uncertainties). Removing this point from the fit yields a gradient of $\Delta[\text{Fe}/\text{H}]/\Delta\log r = -0.45 \pm 0.19$ dex. Both of these values are consistent with the mean gradient found by Geisler *et al.* (1996) of $\Delta[\text{Fe}/\text{H}]/\Delta\log r = -0.4 \pm 0.2$ dex, and the mean gradient found for GCs in general of $\Delta[\text{Fe}/\text{H}]/\Delta\log r = -0.5$ dex (Ashman & Zepf 1998). By comparison, the gradient from the spheroid data of Davies *et al.* (1993) is $\Delta[\text{Fe}/\text{H}]/\Delta\log r = -0.20 \pm 0.10$ dex, similar to the value found by Kim *et al.* (2000) using Washington photometry (for $r \leq 180$ arcsec).

To investigate this matter further, and to directly compare the spheroid light with the globular cluster subpopulations, we have binned our globular clusters into a blue and red population, taking the colour cut to be $C - T_1 = 1.625$. We have further split each of these two bins by radius into two equal components and show our results in Fig. 12.

The Mg_2 and $\langle\text{Fe}\rangle$ indices decrease with increasing galactocentric radius for *both* the red and blue globular cluster subpopulations. Formally, the radial gradients of the clusters from spectroscopy are twice as steep as those determined from the photometric data. However, the significance of this, particularly for the red globular clusters (for which

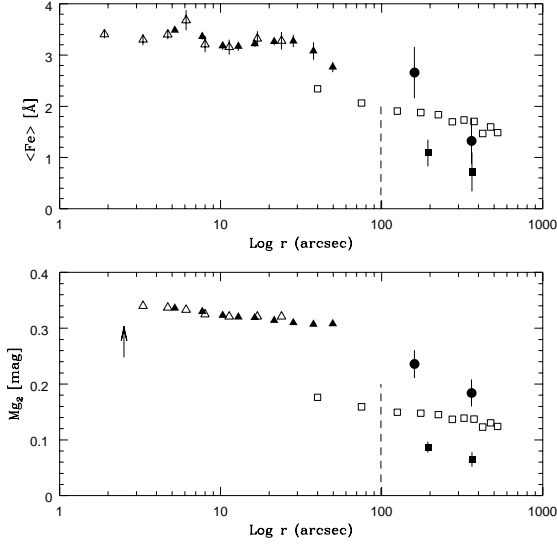


Figure 12. The behaviour of the $\langle \text{Fe} \rangle$ and Mg_2 indices with the logarithm of the galactocentric radius for the two subpopulations of globular clusters. Solid circles represent the red ($C - T_1 \geq 1.625$) globular clusters, solid squares represent the blue globular clusters. The triangles denote the nuclear data of Davies *et al.* (1993), both for the Cryogenic camera (solid) and the Texas Instruments CCD (open triangles). The dashed line indicates the effective radius of NGC 4472. The arrow in the lower panel shows the maximum corrective vector for $[\text{Mg}/\text{Fe}]$ overabundance taken from Henry & Worthey (1999).

$n \sim 23$) is marginal. Measured in $\langle \text{Fe} \rangle$, the innermost red cluster bin is comparable to the spheroid light from Davies *et al.* (1993), whereas the Mg_2 index of this bin is some 0.05 mag lower. In the lower panel of Fig. 12, we plot a vector corresponding to the maximum correction expected for $[\text{Mg}/\text{Fe}]$ overabundant ratios seen in the brightest elliptical galaxies, of which NGC 4472 is known to be affected (Worthey *et al.* 1992; Henry & Worthey 1999; Kobayashi & Arimoto 1999). If we apply this maximum correction (~ 0.05 mag) to the Mg_2 index of the GCs, then these data become consistent with the spheroid data of Davies *et al.* (1993). Since the $\langle \text{Fe} \rangle$ index of the globular clusters is consistent with that of the spheroid light with no correction, we tentatively conclude that the globular clusters in NGC 4472 show no sign of non-solar $[\text{Mg}/\text{Fe}]$ ratios. We return to this point in §5.4.

5.4 Cluster Ages

We now turn to the problem of deriving mean ages for our globular clusters using the Worthey (1994) models. Our primary age indicator for these data is the $H\beta$ index, therefore the uncertainties in this index will reflect heavily on our age estimates for the globular clusters. We calibrate the models to the canonical age we have chosen for the GGCs, which is 12 Gyr. This age for the GGCs is consistent with recent work using the latest HIPPARCOS parallaxes by Carretta *et al.* (2000), and is convenient since this age-line is directly modelled (i.e. not interpolated) by Worthey (1994). We fit the 12 Gyr line of the models to the $H\beta$ index of the GGCs using a χ^2 procedure. The shift implied in $H\beta$ is then applied to

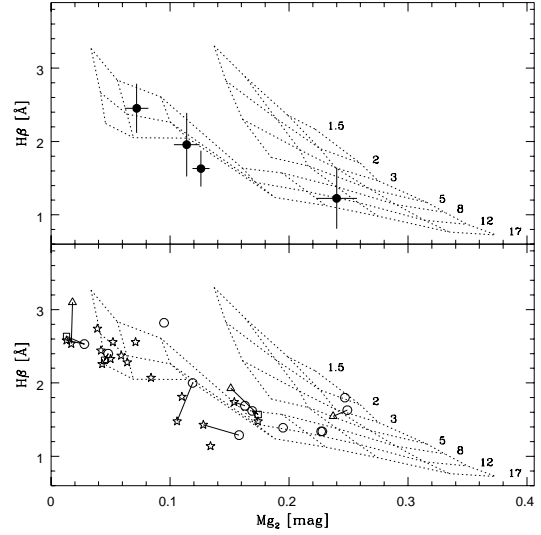


Figure 13. Predictions of the Worthey (1994) models for these data. Top panel: our co-added NGC 4472 GCs are represented by filled circles with error bars. Lower panel: data for the combined sample of GGCs. Open circles are GGCs from Cohen *et al.* (1998), open stars are data from Brodie & Huchra (1990), triangles are our CFHT data and squares are our WHT data. Lines connect the same GGCs between different datasets. The scale on the right side of the grid gives age predictions of the models ranging from 1.5 – 17 Gyr.

our NGC 4472 globular cluster data. This correction to the models is typically ~ -0.4 Å, larger than modelling uncertainties, and is effectively a zero-point calibration. Without this shift, nearly *all* the GGCs would be predicted to have ages ≥ 18 Gyr.

We compare our data to the corrected models in Figs. (13 – 16), each of which consist of two panels: the upper panel over-plots the SSP grids of Worthey (1994) on to our co-added data (filled circles with bootstrapped uncertainties). The lower panel compares the combined sample of GGCs to these same models.

On the whole, the models give a good reproduction of the behaviour of our data, both for the co-added NGC 4472 globular clusters and the GGCs. The Balmer indices track the isochrones of the models fairly closely, across two decades in metallicity. The new modelling of the cluster HBs shows strikingly similar behaviour to that of our three most metal-poor cluster bins. It is apparent that there are small shifts between different metal indices, but these are typically 0.2 Å and well within the uncertainties.

In Fig. 16 we plot $\text{Fe}5270$ against Mg_2 for our data and the combined sample of GGCs. For comparison, we also plot the nuclear data of Davies *et al.* (1993), which we have placed into three radial bins. The spheroid data of Davies *et al.* (1993) is clearly offset from the models, which is usually interpreted as an Mg_2 overabundance (Davies *et al.* 1993). Unlike the stellar spheroid light, the NGC 4472 globular clusters show no evidence of Mg_2 enhancement over iron. This is consistent with the discussion of radial gradients in § 5.3.2

We have already derived metallicities for the GGCs and

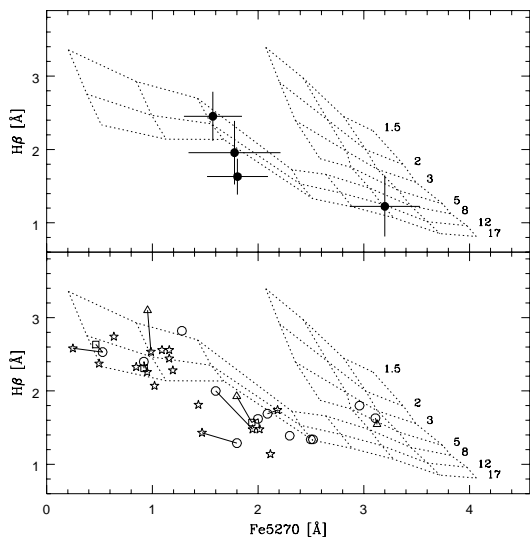


Figure 14. $H\beta$ index against Fe5270. Symbols are the same as for Fig 13.

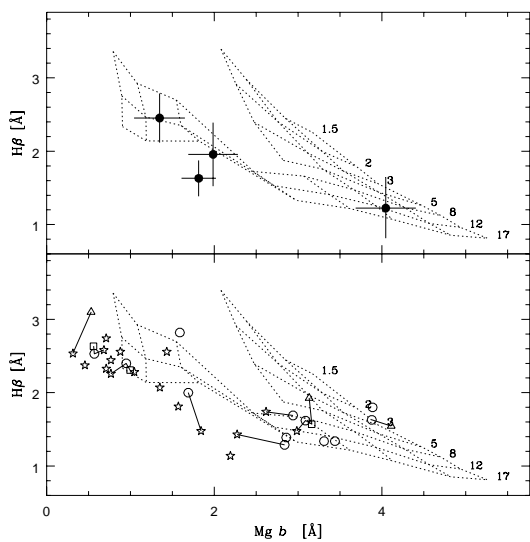


Figure 15. $H\beta$ index versus $Mg\ b$. Symbols are the same as for Fig 13.

NGC 4472 globular clusters, and effectively calculate age as a function of this metallicity since the $H\beta$ (age) lines of the models are calculated with respect to the metal indices. Ages for the NGC 4472 globular clusters are determined using the isochrones of the Worthey (1994) models predicted for the Fe5270, Mg_2 , $Mg\ b$ and $H\beta$ indices along with their respective uncertainties. Our final ages for the co-added globular clusters are the mean age derived from these indices, and are given in Table 9 along with our final metallicities for each bin. In view of the large formal uncertainties, it is clear from Table 9 that there is no evidence of a substantially younger population of globular clusters present in our data. The most metal-rich and metal poor bins appear to be younger than the two intermediate ones. This is likely an artefact of the

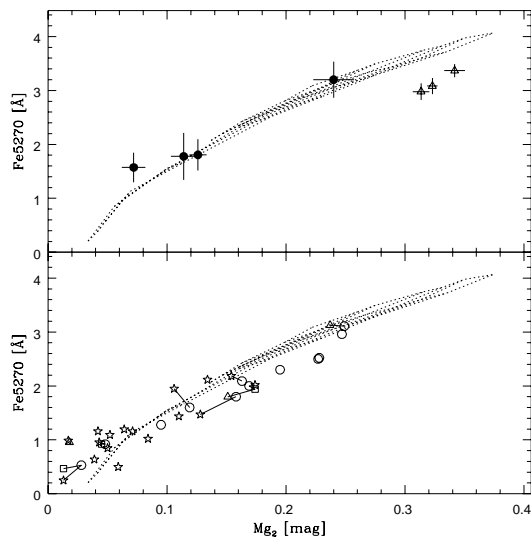


Figure 16. Fe5270 index versus Mg_2 . Symbols same as Fig 13, but also including the spheroid data of Davies *et al.* (1993) which we have binned in radius (open triangles, top panel). The age scale of the models has been omitted for clarity.

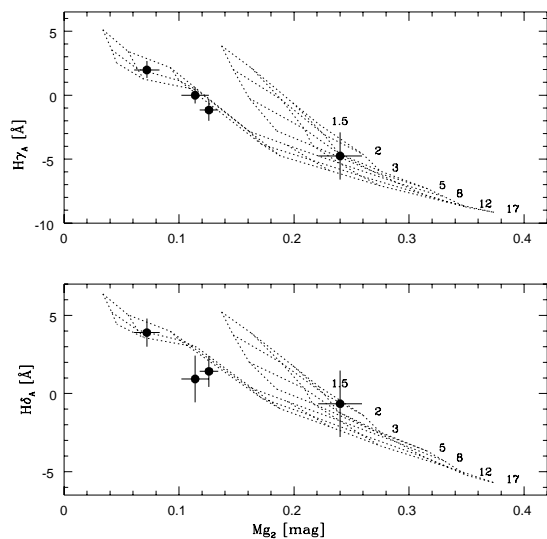


Figure 17. The Worthey (1994) model predictions for our two other age indicators. Top panel: $H\gamma_A$ versus Mg_2 , bottom panel: $H\delta_A$ versus Mg_2 .

Worthey (1994) models at metallicities $-1.0 < [Fe/H] < -0.5$, the regime where HB morphology starts to play a role. The switch to M3 morphology happens below $[Fe/H] = -0.95$ and the switch to M92 morphology happens below $[Fe/H] = -1.55$. This change does not occur as a smoothly varying function of metallicity, and therefore may be predicting too sharp a rise in the $H\beta$ index. The models also predict too old an age for the GGCs at these metallicities. Since the 12 Gyr age isochrone of the models is fit to the GGCs, this may have the effect of inducing too large a shift in $H\beta$ and therefore predicting younger ages in the co-added data. Formally,

Table 9. The final ages and metallicities for our co-added data, derived from the stellar population models of Worthey (1994). The final ages in column 3 are the mean of those predicted by the $H\beta$ index as a function of Fe5270, Mg b and Mg₂.

Bin #	[Fe/H] _Z (dex)	Mean Age (Gyr)
1	-1.29 ± 0.30	10.7^{+6}_{-5}
2	-0.91 ± 0.35	15.3^{+6}_{-5}
3	-0.84 ± 0.25	18.5^{+4}_{-5}
4	-0.27 ± 0.30	11.3^{+8}_{-9}

the mean age of the four bins is 14 ± 6 Gyr, consistent with our canonical age adopted for the GGCs of 12 Gyr.

We have also measured two other primarily age-sensitive indices, namely $H\gamma_A$ and $H\delta_A$, which we show in Fig. 17. Both these indices exhibit similar behaviour to $H\beta$ measured for the globular clusters, but with indications that the most metal-rich bin is somewhat younger than the others. However, not only is the correction of the models to these data more uncertain (since we have few GGCs for which there are $H\gamma_A$ and $H\delta_A$ measurements), but also the uncertainties in these indices are somewhat larger, and therefore we do not derive ages for the globular clusters from these higher-order Balmer lines.

In order to reduce the uncertainties in the indices (especially $H\beta$), but at the expense of losing our baseline in metallicity, we have also binned our sample of NGC 4472 globular clusters into one metal-poor globular cluster population and one metal-rich population. We take the dividing line between the populations as $C - T_1 = 1.625$, obtained from the KMM mixture-modelling test (Ashman *et al.* 1994) applied to the full NGC 4472 globular cluster data of Geisler *et al.* (1996). Again we co-add these data and measure the Lick/IDS indices using the bootstrap procedure described previously. Our metal-poor and metal-rich bins contain 85 and 45 spectra respectively, with flux weighted colours of $C - T_1 = 1.4$ and $C - T_1 = 1.8$, corresponding to metallicities of $[\text{Fe}/\text{H}] = -1.10$ and $[\text{Fe}/\text{H}] = -0.16$ using Eqn. (4). We plot Mg b , Fe5270 and Mg₂ against $H\beta$ for these bins in Fig. 18. Again, the models have been normalised to the canonical ages adopted for the GGCs. From these indices, we obtain a mean age of 14.5 ± 4 Gyr for the metal-poor bin and 13.8 ± 6 Gyr for the metal-rich bin. The smaller uncertainties in the metal-poor bin correspond to the larger numbers of blue globular cluster spectra available for co-addition (for $40 \leq n \leq 100$ the uncertainty in the index goes as $\sigma \propto n^{-0.3}$).

As a check for systematic errors in our age results, we perform Monte Carlo simulations on the Worthey (1994) model SEDs predicted for the ages and metallicities of our metal-poor and metal-rich globular cluster bins. We obtain SEDs corresponding to the indices measured for each bin and then artificially degrade them following a procedure similar to that described in § 4.2. We generate the same number of realisations as there are spectra in each of our red and blue bins. We then measure the ages of the co-added artificial spectra, again using the Worthey (1994) grids. We find that each of our cluster bins is older than 6 Gyr at the

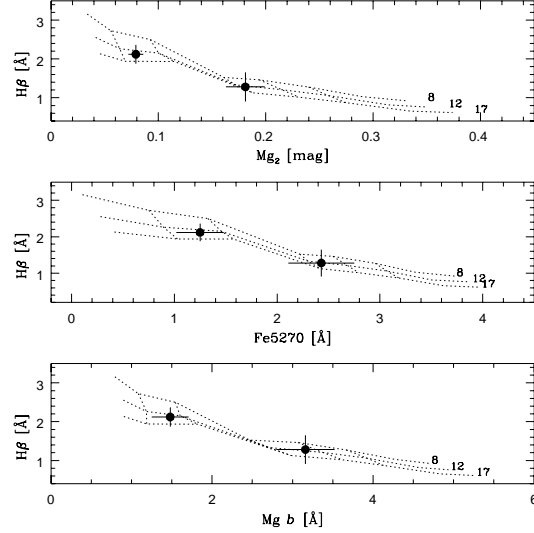


Figure 18. Age predictions of the Worthey (1994) models for the $H\beta$ index versus Mg₂, Fe5270 and Mg b for our metal-poor and metal-rich bins of NGC 4472 globular clusters. We show only the $\tau \geq 8$ Gyr isochrones for clarity.

95 % confidence level, and older than 3 Gyr at the 98.5 % confidence level.

From HST V and I data, Puzia *et al.* (1999) find that the red and blue GCs in NGC 4472 are old and coeval within their errors, but that formally the *blue* GCs are somewhat younger. Lee & Kim (2000) conclude that the *red* GCs are younger than the blue by 'several' Gyr from the same data (plus one additional HST field), attributing their differences to a larger sample size, increased areal coverage and greater completeness.

Our findings that the blue and red globular clusters of NGC 4472 are old and coeval within the uncertainties (but formally the red GCs are younger) are not inconsistent with either of the above two studies, but do not rely on any assumption about the underlying mass distributions of the globular cluster populations.

6 DISCUSSION

The major conclusions of this work are that the NGC 4472 globular cluster subpopulations are essentially coeval and old, and separated by ~ 1.0 dex in $[\text{Fe}/\text{H}]$. The NGC 4472 GCS exhibits a radial metallicity gradient steeper than the underlying halo light of the galaxy, with the red and blue globular clusters both showing some evidence of this behaviour. The globular cluster populations of NGC 4472 clearly formed from gas with significantly different levels (perhaps histories) of enrichment, but at roughly similar times. A strong radial metallicity gradient in the globular clusters would imply a largely dissipative formation mechanism, which classically points toward some form of monolithic protogalactic collapse (e.g. Eggen, Lynden-Bell & Sandage 1962), or modified multiphase collapse model (e.g. Forbes, Brodie & Grillmair 1997). A gradient of $\Delta[\text{Fe}/\text{H}]/\Delta \log r \simeq -0.4$ for the GCs is well within the predictions of the-

oretical models of the formation of spheroids. For example, the dissipative models of Larson (1974) predict $\Delta[\text{Fe}/\text{H}]/\Delta \log r = -1.0$, whilst the variants of Carlberg (1984) range from -0.5 to 0.0 . However, these models lead to large rotation at high metallicity, which is not observed for this galaxy (e.g. Zepf *et al.* in preparation). Large radial gradients also do not preclude the possibility that major mergers may have contributed to the formation of NGC 4472 and its GCS (e.g. Ashman & Zepf 1992). As simulations show (e.g. White 1980; Barnes 1988), a radial gradient is not necessarily destroyed during the merger of disks, but may simply become somewhat diluted.

In terms of abundance ratios, the variation seen in $[\text{Mg}/\text{Fe}]$ is generally attributed to different levels of enrichment from Type Ia (largely contributing Fe) and Type II (Mg and Fe with all other elements) supernovae. If the NGC 4472 globular clusters truly possess $[\text{Mg}/\text{Fe}] \simeq 0$, then this would imply that their formation was decoupled (at some level) from that of the spheroid light. Whether differing degrees of Type Ia/Type II enrichment indicates different star formation time-scales, a variable binary fraction or a variable IMF is uncertain. But certainly determining whether the $[\alpha/\text{Fe}]$ ratios in globular clusters are truly enhanced with respect to solar, and whether there are variations *between* different cluster subpopulations will place strong constraints on their formation.

Measuring age differences between old stellar populations is notoriously difficult. Indeed if the metal-poor and metal-rich globular clusters really *are* separated in age by several Gyr, how may we proceed to detect this difference? The automatic response from this work would be to state that better quality, high S/N spectra of individual globular clusters are required for accurate age-dating. One step would be to move away from instrument-specific systems which often require many correction factors and the degradation in resolution of ones data. This is effectively throwing away information, a better route perhaps is followed by Vazdekis *et al.* (1996) whereby the models are freely available to be adapted to the characteristics of these data, in order to maximize the information obtained from these data. Globular clusters are essentially homogeneous and coeval associations of stars, and therefore the assumptions implicit in SSP models are well suited to these systems. The fact that observed ages and metallicities are luminosity-weighted is less significant for globular clusters, unlike the situation for composite stellar systems (i.e. galaxies) whose integrated light may be dominated by the most recent star formation event. It is unfortunate then, that the sub-solar regime of the models (the parameter space of the majority of globular clusters) is poorly constrained. At the most metal-poor end, SSP model grids are uncertain by many Gyr for a given measurement of $H\beta$. This largely stems from the lack of metal-poor stars in the solar neighbourhood, and the assumptions made for HB morphology. Moreover, the SSP models are based upon stellar libraries of stars of solar abundance ratios, whereas the abundances of the most luminous ellipticals are clearly non-solar (e.g. Worthey *et al.* 1992). Abundances obtained from α -elements are typically much higher than those derived from the iron-peak, and this is the principle reason for uncertainty in the absolute abundance and age scales.

Spectroscopy is the only way of unambiguously identifying *bona fide* globular clusters (through their kinematics),

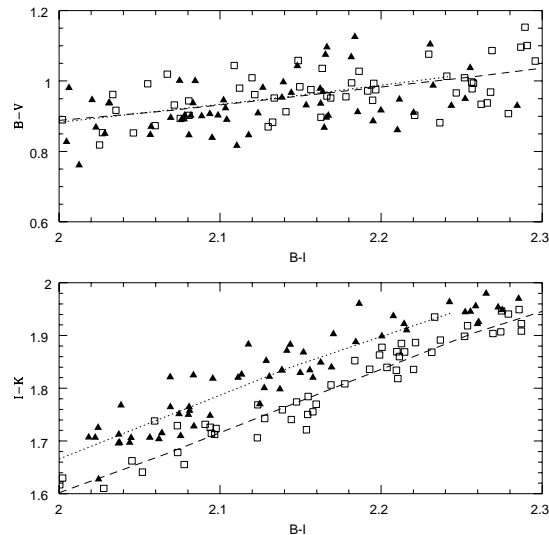


Figure 19. The predicted B , V , I and K colours for a subset of NGC 4472 globular clusters (Geisler *et al.* 1996) using the stellar population models of Vazdekis (in preparation). Solid triangles represent the red ($C - T_1 \geq 1.625$) globular clusters, with an assumed age of 10 Gyr, open squares represent the blue globular clusters, with an assumed age of 15 Gyr. We have included a representative observational scatter of 0.05 mag in the colours. The top panel highlights the degeneracy between age and metallicity in optical broadband colours, whereas the inclusion of the K -band (lower panel) can distinguish between the two cluster populations. Dashed and dotted lines indicate the 15 Gyr and 10 Gyr isochrones of the models respectively.

in addition to investigating α -element enhancement. However, building up statistically significant samples of high S/N spectra for globular clusters is time consuming, even on 8-metre class telescopes. An alternative route towards disentangling the ages and metallicities for globular clusters is through the use of two colour photometry, with the inclusion of an infrared passband (Kissler-Patig 2000). SSP models of broadband optical colours are effectively degenerate, and isochrones in these models ranging from 1 – 17 Gyr are largely superposed upon lines of constant metallicity. However, a colour such as $I - K$ directly measures the temperature of the red giant branch in old stellar populations, which is dependent almost entirely on metallicity. By plotting a metallicity sensitive colour against an age/metallicity sensitive colour allows the extraction of age information (albeit still requiring high photometric accuracy, $\simeq 0.05$ mag). Fig 19 illustrates the effect of including the K -band in two-colour SSP model predictions. We have taken a subset of ~ 300 globular clusters from the catalogue of Geisler *et al.* (1996), and have assigned the blue globular clusters an age of 15 Gyr, and the red ($C - T_1 \geq 1.625$) globular clusters an age of 10 Gyr. We then plot the predictions of the SSP models of Vazdekis (in preparation) for the B , V , I and K bands at these ages and metallicities, including an observational uncertainty of 0.05 mag in the colours. The optical colours are clearly degenerate, but the inclusion of the K -band provides a powerful discriminant between age and metallicity.

7 SUMMARY

We have derived ages and metallicities from 130 co-added globular cluster spectra associated with the giant elliptical NGC 4472. We have measured metallicity sensitive and age sensitive line indices from the spectra and compared them to the stellar population models of Worthey (1994). We find that the globular clusters span a metallicity range of approximately $-1.6 \leq [\text{Fe}/\text{H}] \leq 0$ dex, corresponding to the range covered by the more metal-rich two-thirds of the Milky Way globular cluster system. Although absolute ages are uncertain, via the calibration of the stellar population models with Galactic Globular Clusters, we find that the metal-poor population of NGC 4472 globular clusters has an age of 14.5 ± 4 Gyr, whilst the metal-rich population is 13.8 ± 6 Gyr old. Monte Carlo simulations indicate that both the globular cluster populations present in these data are older than $\tau = 6$ Gyr at the 95 % confidence level. The NGC 4472 globular cluster system exhibits a radial metallicity gradient steeper than the underlying spheroid light of the galaxy even after correction for the varying spatial distribution of the blue and red globular cluster populations. We see no evidence for non-solar $[\text{Mg}/\text{Fe}]$ ratios for the higher metallicity globular clusters, at the level observed for the spheroid light. This would indicate that the formation of the NGC 4472 globular clusters was probably decoupled from that of the spheroid stars.

8 ACKNOWLEDGEMENTS

MB would like to acknowledge Guy Worthey and Alexandre Vazdekis for the use of their stellar population models, and PPARC for its supporting studentship. Thanks also go to Harald Kuntschner and John Blakeslee, who both provided useful comments regarding this paper, and the referee, Raffaele Gratton, for his perceptive reading of the paper. MB also acknowledges the use of the STARLINK facilities at the University of Durham.

REFERENCES

- Aaronson M., Cohen J.G., Mould J., Malkan M., 1978, *ApJ*, 223, 824
- Armandroff T.E., Zinn R.J., 1988, *AJ*, 96, 92
- Ashman K.M., Zepf S.E., 1992, *ApJ*, 384, 50
- Ashman K.M., Bird C.M., Zepf S.E., 1994, 108, 2348
- Ashman K.M., Zepf S.E., 1998, *Globular Cluster Systems*, eds., King A., Lin D., Maran S., Pringle J., Ward M., Cambridge University Press
- Barnes J.E., 1988, *ApJ*, 331, 699
- Brodie J.P., Huchra J.P., 1990, *ApJ*, 362, 503
- Brodie J.P., Huchra J.P., 1991, *ApJ*, 379, 157
- Burstein D., Faber S.M., Gaskell C.M., Krumm N., 1984, *ApJ*, 287, 586
- Carlberg R.G., 1984, *ApJ*, 286, 403
- Carretta E., Gratton R.G., 1997, *A&AS*, 121, 95
- Carretta E., Gratton R.G., Clementini G., Fusi-Peccini F., 2000, *ApJ*, 533, 215
- Cohen J.G., 1988, *AJ*, 95, 982
- Cohen J.G., Blakeslee J.P., Ryzhov A., 1998, *AJ*, 496, 808
- Couture J., Harris W.E., Allwright J.W.B., 1991, *ApJ*, 372, 97
- Davies R.L., Sadler E.M., Peletier R.F., 1993, *MNRAS*, 262, 650
- Eggen O.J., Lynden-Bell D., Sandage A.R., 1962, *ApJ*, 136, 748
- Faber S.M., 1972, *A&A*, 20, 361
- Faber S.M., Friel E. D., Burstein D., Gaskell C. M., 1985, *ApJS*, 57, 711
- Forbes D.A., Brodie J.P., Grillmair C.J., 1997, *AJ*, 133, 1652
- Gebhardt K., Kissler-Patig M., 1999, *AJ*, 118, 1526
- Geisler D., Forte J.C., 1990, *ApJ*, 350, 5
- Geisler D., Lee M.G., Kim E., 1996, *AJ*, 111, 1529
- González J.J., 1993, PhD thesis, University of California, Santa Cruz
- Gorgas J., Faber S.M., Burstein D., González J.J., Courteau S., Prosser C., 1993, *ApJS*, 86, 153
- Hanes D.A., Brodie J.P., 1986, *ApJ*, 300, 279
- Harris H.C., Canterna R., 1977, *AJ*, 82, 798
- Harris G.L.H., Geisler D., Harris H.C., Hesser J.E., 1992, *AJ*, 104, 613
- Henry R.B.C., Worthey G., 1999, *PASP*, 111, 919
- Kim E., Lee M.G., Geisler D., 2000, in press, astro-ph/0001007
- Kissler-Patig M., 2000, astro-ph/0002070
- Kissler-Patig M., Brodie J.P., Schroder L.L., Forbes D.A., Grillmair C.J., Huchra J.P., 1998, *AJ*, 115, 105
- Kobayashi C., Arimoto N., 1999, *AJ*, 527, 573
- Kundu A., Whitmore B.C., Sparks W.B., Macchetto F.B., Zepf S.E., Ashman K.E., 1999, *ApJ*, 513, 733
- Larson R.B., 1974, *MNRAS*, 166, 585
- Lee M.G., Kim E., 2000, astro-ph/0004116
- Lee M.G., Kim E., Geisler D., 1998, *AJ*, 115, 947
- Meylan G., Heggie D.C., 1997, *Astron. Astrophys. Rev.*, 8, 1
- Mould J.R., Oke J.B., de Zeeuw P.T., Nemeč J.M., 1990, *AJ*, 99, 1823
- Neilsen E.H., Tsvetanov Z.I., 1999, *ApJ*, 515, 13
- O'Connell R.W., 1976, *ApJ*, 206, 370
- Puzia T.H., Kissler-Patig M., Brodie J.P., Huchra J.P., 1999, *AJ*, 118, 2734
- Sandage A., Tammann G.A., 1981, *A Revised Shapley-Ames Catalogue of Bright Galaxies* (Washington : Carnegie Inst. Washington)
- Sharples R.M., Zepf S.E., Bridges T.J., Hanes D.A., Carter D., Ashman K.M., Geisler D., 1998, *AJ*, 115, 2337
- Tonry J., Davis M., 1979, *AJ*, 84, 151
- Vazdekis A., Casuso E., Peletier R.F., Beckman J.E., 1996, *ApJS*, 106, 307
- White S.D.M., 1980, *MNRAS*, 191, 1
- Worthey G., Faber S.M., González J.J., 1992, *AJ*, 398, 69
- Worthey G., 1993, *ApJ Lett.*, 415, L91

- Worthey G., 1994, ApJS, 95, 107
Worthey G., Ottaviani D.L., 1997, ApJS, 111, 377
Worthey G., Faber S.M., González J.J., Burstein D., 1994, ApJS,
94, 687
Zepf S.E., Ashman K.M., 1993, MNRAS, 264, 611
Zepf S.E., Ashman K.M., English J., Freeman K.C., Sharples
R.M. 1999, AJ, 118, 752
Zinn R. 1985, ApJ, 293, 424